

Noise classification in small quantum networks by Machine Learning

Shreyasi Mukherjee¹, Dario Penna², Fabio Cirinnà², Mauro Paternostro^{3,4}, Elisabetta Paladino^{1,5,6}, Giuseppe Falci^{1,5,6}, and Luigi Giannelli^{1,5}

¹ Dipartimento di Fisica e Astronomia “Ettore Majorana”, Università di Catania, Via S. Sofia 64, 95123 Catania, Italy

² Leonardo S.p.A., Cyber & Security Solutions, 95121, Catania, Italy

³ Università degli Studi di Palermo, Dipartimento di Fisica e Chimica - Emilio Segrè, via Archirafi 36, I-90123 Palermo, Italy

⁴ Centre for Theoretical Atomic, Molecular, and Optical Physics, School of Mathematics and Physics, Queens University, Belfast BT7 1NN, United Kingdom

⁵ INFN, Sezione di Catania, 95123, Catania, Italy

⁶ CNR-IMM, UoS Università, 95123, Catania, Italy

Abstract. We investigate machine learning-based noise classification aimed at the recognition of the Markovian character of a dynamics and the identification of correlations of classical noise, as well as their interplay in small quantum networks. We operate control based on Coherent Tunneling by Adiabatic Passage (CTAP) or Stimulated Raman Adiabatic Passage (STIRAP) in a three-level system using different pulse configurations as inputs to train a feedforward neural network. Our results show that supervised learning can classify distinct types of classical diagonal noise affecting the system. Three non-Markovian (quasistatic correlated, anti-correlated, and uncorrelated) and Markovian noise mechanisms are classified with 99% accuracy. Instead, correlations of Markovian noises cannot be classified with our method. The approach is robust against statistical measurement errors keeping its effectiveness even for physical measurements where a limited number of samples is available.

1. Introduction

Quantum systems can nowadays be controlled with impressive accuracy [1] to perform new tasks leveraging their coherence properties, such as superposition and entanglement [2]. However, quantum behavior fades away because of environmental noise leading to loss of fidelity in quantum operations and decoherence [3–5]. Devising strategies to counteract these effects is thus paramount for advances in quantum technologies and in this context, machine learning (ML) emerges as an innovative and powerful diagnostic tool [6–8]. Approaches based on ML have been applied to various quantum control protocols [9–12], to quantum state tomography [13–15], to characterize quantum systems [16–18], to simulate open quantum systems [13, 18–20], to investigate

non-Markovian dynamics [21, 22] and, in a spirit similar to this work, to characterize system-environment interactions [23, 24] and perform noise spectroscopy [25–27].

Mitigating decoherence effects is necessary to achieve quantum advantage. Several strategies have been developed in the last two decades both for quantum computation and in the broader perspective of quantum control. Error-avoidance (or passive stabilization) strategies consist of storing and processing information in suitably designed subspaces of the Hilbert space, which are protected from the interaction with the environment [28–30]. Examples of error-correcting (or active stabilization) strategies are Quantum Error Correction which relies on non-local information encoding [5, 31, 32], and Dynamical Decoupling [30, 33–35] consisting in repeated application of pulsed or switched control which has been used in solid-state coherent nanoscience to counteract $1/f$ noise [28, 36–38]. Specific strategies rely on the availability of information about the environment, whose characterization is thus a very important step towards the design of optimized systems and protocols. For individual qubits, this program has been carried out successfully in several platforms such as trapped ions [39, 40], photonic qubits [41], nuclear magnetic resonance [42, 43], and nitrogen-vacancy centres in diamond [44, 45]. Superconducting systems are the forefront examples in this context, with decoherence times that have improved from a few nanoseconds to milliseconds in about 15 years [46].

On the contrary, characterization of more complex systems such as multilevel nodes and multi-qubit architectures is still a challenge. In particular, the need of characterizing correlations between noises affecting different transition [47] or different nodes of the quantum architecture [48] is an emerging issue. A strong motivation of principle is that spatially correlated noise between physical qubits may spoil one of the pillars of digital quantum computation namely error correction in logical qubits, besides the fact that correlated errors are indeed observed in noisy intermediate-scale quantum structures [49]. Effects of spatially-correlated low-frequency noise between two quantum devices have been observed since several decades [50] and their impact on decoherence was investigated [48] since the first two-qubit superconducting gates were demonstrated. Recently, low-frequency noise correlations between pairs of qubits have been characterized by direct measurement of the noise power spectra [51–53]. However, the full characterization of noise acting on a controllable quantum system is a difficult task requiring exceedingly large resources as the systems scale up. In this work, we seek to pursue a different avenue passing through the classification of the multivariable noise acting on a quantum architecture. Our primary focus is to find a ML-based procedure that recognizes the presence of noise correlations. We will see that this possibility is intimately related to the (non-)Markovian character of the dynamics, and might thus be useful in the investigation of the effect that non-Markovianity has in the establishment of many-body phenomena [54, 55].

For the sake of simplicity, we illustrate our ML method to identify correlations in the simplest case of a three-level network affected by diagonal classical noise. Physically, the model describes a qutrit operated by two AC classical electromagnetic fields or a system of three single-level quantum dots with tunable tunneling rate. In the latter

case, we exploit a control protocol yielding coherent tunneling by adiabatic passage (CTAP) [56], which is conventionally meant to be used for population transfer, as a tool for noise classification. We use supervised learning to classify five types of noise:

- (1) Non-Markovian correlated noise;
- (2) Non-Markovian anti-correlated noise;
- (3) Non-Markovian uncorrelated noise;
- (4a) Markovian correlated noise;
- (4b) Markovian anti-correlated noise.

We show that, by measuring the efficiency of CTAP under three different combinations of pulse amplitudes, we can train a neural network to classify noise belonging to four of the five classes listed above. In particular, our model can accurately classify noise of the first three classes and Markovian noise (classes 4a and 4b together) while it cannot distinguish between correlated and anti-correlated Markovian noise. Referring to actual experiments, we analyze in detail how to extract this information also in the case of a finite number of samples.

The paper is structured as follows: in Sec. 2 we define the models of system and noise that we address in our study. In Sec. 3 we introduce the CTAP protocol and the figures of merits we use in the training phase. In Sec. 4 we give a brief overview of *supervised learning* and *neural networks* (NN) [6, 57–59] and describe how we classify among the noises introduced in Sect. 2. Sec. 5 presents the results on the classification for a finite number of samples and imperfect measurements. The conclusions are drawn in Sec. 7, together with a physical interpretation of the results.

2. Noisy three-level system

To fix the ideas we consider a system of three single-level quantum nodes with eigenbasis $\{|i\rangle, i = 0, 1, 2\}$ and on-site energies ϵ_i . This model may describe a system of three quantum dots with an electron tunneling between them [56]. The tunneling rates between the first and the second dot, $\Omega_p(t)$, and between the second and the third dot, $\Omega_s(t)$, can be controlled by time-dependent external gates. The same model describes a three-level atom driven by two external fields in a multiple rotating frame [60].

The Hamiltonian of the system is $H_{\text{sys}} = H_0 + H_c$, where H_0 and $H_c(t)$ are the free energy and the control term, respectively (throughout the manuscript we use units such that $\hbar = 1$), reading

$$H_0 = \delta_p |1\rangle\langle 1| + \delta |2\rangle\langle 2|, \quad (1a)$$

$$H_c = \frac{\Omega_p(t)}{2} (|0\rangle\langle 1| + |1\rangle\langle 0|) + \frac{\Omega_s(t)}{2} (|1\rangle\langle 2| + |2\rangle\langle 1|), \quad (1b)$$

where, in the language of the three-dot network, we defined the *detunings* $\delta_p = \epsilon_1 - \epsilon_0$ and $\delta = \epsilon_2 - \epsilon_0$.

We consider diagonal noise, i.e. noise affecting the energy levels of the three dots, which may arise from charge noise, for instance [61]. We model it as the following classical stochastic process added to the diagonal entries of the Hamiltonian

$$H_{\text{noise}} = \tilde{x}_1(t)|1\rangle\langle 1| + \tilde{x}_2(t)|2\rangle\langle 2|. \quad (2)$$

Here, $\tilde{x}_i(t)$ ($i = 1, 2$) is a random variable [62] with normalized probability density $p(x_i, t)$. The total Hamiltonian $H(t)$ in the basis $\{|0\rangle, |1\rangle, |2\rangle\}$ thus reads

$$H(t) = H_{\text{sys}}(t) + H_{\text{noise}}(t) = \begin{pmatrix} 0 & \Omega_p(t)/2 & 0 \\ \Omega_p(t)/2 & \delta_p + \tilde{x}_1(t) & \Omega_s(t)/2 \\ 0 & \Omega_s(t)/2 & \delta + \tilde{x}_2(t) \end{pmatrix}. \quad (3)$$

We now link the five classes of noise listed in Sec. 1 to the features of the stochastic mechanism introduced here. We thus consider

- **Non-Markovian types of noise:** When addressing non-Markovian noise, we will make the assumption of *quasistatic processes* where the noise mechanism has a long correlation time and can thus be considered constant over the evolution of the system. The random variables $\tilde{x}_i(t)$ are assumed to be picked from Gaussian distributions with zero mean, thus describing the cumulative effects of independent microscopic sources. Needless to say, while $\tilde{x}_i(t)$ remains constant throughout a single realization of the protocol, it varies between different realizations. We identify the following three classes
 - (1) Correlated: $x_2(t) = \eta x_1(t)$ with $\eta > 0$;
 - (2) Anti-correlated: $x_2(t) = \eta x_1(t)$ with $\eta < 0$;
 - (3) Uncorrelated: $x_2(t)$ and $x_1(t)$, are independent of each other.
- **Markovian types of noise:** The associated dynamics will be ruled by zero-mean, delta-correlated stochastic processes \tilde{x}_i making the dynamics of the system dependent only on its current state rather than its past history. We will thus set

$$\langle \tilde{x}_i(t) \rangle = 0, \quad \langle \tilde{x}_i(t) \tilde{x}_i(t') \rangle = \gamma \delta(t - t') \quad (4)$$

and consider the two classes

- (4a) Correlated: $x_2(t) = \eta x_1(t)$, with $\eta > 0$;
- (4b) Anti-correlated: $x_2(t) = \eta x_1(t)$, with $\eta < 0$.

3. Dynamics

Our method is based on population transfer by CTAP and the closely related stimulated Raman adiabatic passage (STIRAP) scheme, which has found ample use in atomic physics [60, 63]. We shortly review the CTAP/STIRAP approaches and discuss how we solve the equations and then calculate the classification performances in the presence of the different classes of noise considered.

3.1. CTAP/STIRAP

CTAP [56] (and its spin equivalent spin-CTAP [64]) is a protocol that ideally achieves population transfer from $|0\rangle$ to $|2\rangle$ by adiabatically following a “trapped state” (often referred to as a dark state) that contains no contribution from the intermediate state $|1\rangle$, which is thus never populated during the protocol. Under ideal conditions, CTAP/STIRAP yields $\sim 100\%$ -efficiency population transfer with remarkable robustness against parametric fluctuations and state-selectivity.

For the transfer process to be successful it is essential to work at small detuning, $\delta \ll \Omega_{p,s}$. In particular, at the so-called two-photon resonance condition $\delta = 0$, the trapped state is an instantaneous eigenstate of the Hamiltonian $H_{\text{sys}}(t)$ of the form

$$|\phi_{\text{D}}(t)\rangle = \cos \theta(t)|0\rangle - \sin \theta(t)|2\rangle \quad (5)$$

with $\theta(t) = \tan^{-1} [\Omega_{\text{p}}(t)/\Omega_{\text{s}}(t)]$. The protocol is operated in the time interval $[t_i, t_f]$ by applying pulses $\Omega_{p,s}(t)$ in a *counterintuitive* manner [60]: Ω_{s} is applied *before* Ω_{p} , while ensuring that the two pulses overlap in a fraction of the duration of the sequence. In this case, the trapped state $|\phi_{\text{D}}(t)\rangle$ at the initial time t_i coincides with $|0\rangle$ and at the final time t_f with the target state $|2\rangle$. If the evolution is adiabatic and the system is prepared in $|0\rangle = |\phi_{\text{D}}(t_i)\rangle$, the system evolves following the trapped state $|\phi_{\text{D}}(t)\rangle$ throughout the evolution as prescribed by the adiabatic theorem [65, 66]. The requested adiabaticity of the process can be cast in the form of the global adiabaticity condition [60]

$$\Omega_{p/s}^{\max} \tau \geq 10, \quad (6)$$

where τ is the characteristic time scale of the pulses overlap and $\Omega_{p/s}^{\max} = \max_t \Omega_{p/s}(t)$.

Under two-photon resonance condition, a counterintuitive sequence satisfying the global adiabaticity request is robust against the actual shape of Ω_{p} and Ω_{s} . In fact, several pulse shapes [67] have been used in literature. In this work, we consider Gaussian pulses (see Fig. 1) of the form

$$\Omega_{\text{p}}(t) = \Omega_{\text{p}}^{\max} e^{-(\frac{t-\tau}{T})^2}, \quad \Omega_{\text{s}}(t) = \Omega_{\text{s}}^{\max} e^{-(\frac{t+\tau}{T})^2}, \quad (7)$$

and we let the system evolve in the time interval $t \in [-5T, 5T]$ with $\tau = 0.7T$. More details about CTAP/STIRAP can be found in Appendix B.

3.2. Figures of merit

The efficiency ξ of the population transfer is defined as the population of the target state $|2\rangle$ at the final time t_f , averaged over all the possible realizations of the noise [68]

$$\xi = \lim_{N \rightarrow \infty} \frac{1}{N} \sum_{r=1}^N |\langle 2 | \psi^{(r)}(t_f) \rangle|^2 = \lim_{N \rightarrow \infty} \frac{1}{N} \sum_{r=1}^N \xi^{(r)} \quad (8)$$

with $\xi^{(r)} = |\langle 2 | \psi^{(r)}(t_f) \rangle|^2$ the population of $|2\rangle$ for a single trajectory $|\psi^{(r)}(t)\rangle$ identified by an individual realization of noise, i.e. a choice of $\{x_1^{(r)}(t), x_2^{(r)}(t)\}$. The index $r = 1, \dots, N$ identifies the trajectory being considered.

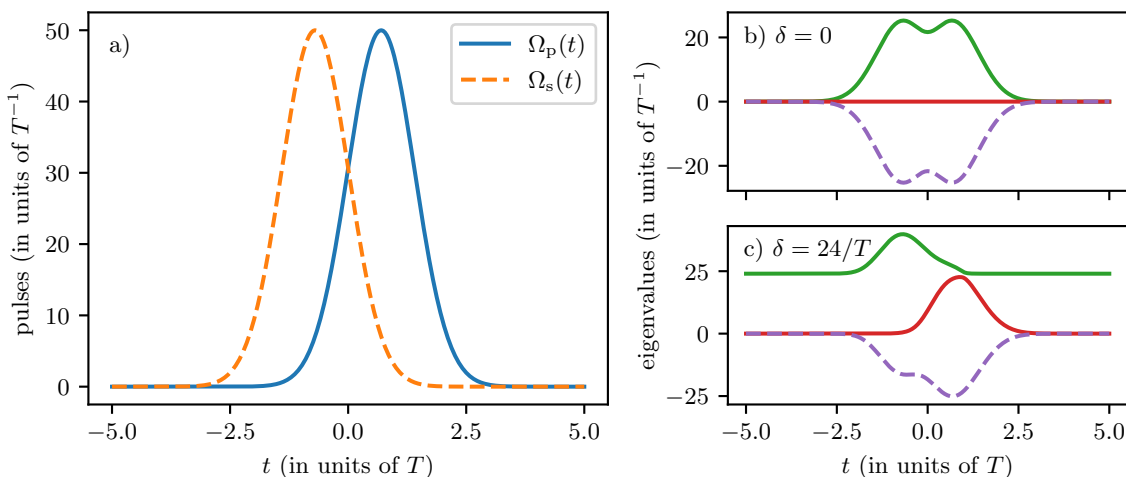


Figure 1. (a) Example of the pump $\Omega_p(t)$ and Stokes $\Omega_s(t)$ pulses, Eqs. (7), as a function of time t . The parameters used are $\Omega_p^{\max} = \Omega_s^{\max} = 50/T$, $\tau = 0.7T$ and $t \in [-5T, 5T]$. (b) Instantaneous eigenvalues for $\delta = 0$: CTAP/STIRAP achieves 100% population transfer by adiabatically following the trapped state $|\Phi_D(t)\rangle$ (red line). (c) Instantaneous eigenvalues for $\delta \neq 0$: The trapped state is not an instantaneous eigestate and an adiabatic evolution produces only partial population transfer.

The quasistatic noise is constant during an individual trajectory thus the index r can be unambiguously mapped to the two real values $x_1^{(r)}$ and $x_2^{(r)}$ of the random processes \tilde{x}_1 and \tilde{x}_2 . Therefore $\xi^{(r)} = \xi(x_1^{(r)}, x_2^{(r)})$. In this case, the efficiency in Eq. (8) is obtained by averaging over the random processes

$$\xi = \int \xi(x_1, x_2) p(x_1, x_2) dx_1 dx_2. \quad (9)$$

If the noise is (anti-)correlated, then $x_2^{(r)} = \eta x_1^{(r)}$ and Eq. 9 simplifies to

$$\xi = \int \xi(x_1, \eta x_1) p_1(x_1) dx_1. \quad (10)$$

For Markovian noise, the average is calculated via the density matrix $\rho(t)$ of the system which solves a master equation in the Lindblad form (cf. Appendix A for the derivation)

$$\dot{\rho}(t) = -i[H_0 + H_c(t), \rho(t)] - \frac{\gamma}{2}(O^2 \rho(t) + \rho(t) O^2 - 2O \rho(t) O), \quad (11)$$

where $O = |1\rangle\langle 1| + \eta|2\rangle\langle 2|$, and γ is the dephasing rate given by $\langle \tilde{x}_1(t) \tilde{x}_1(t') \rangle = \gamma \delta(t - t')$. The efficiency is given by

$$\xi = \langle 2 | \rho(t_f) | 2 \rangle. \quad (12)$$

4. Classification with neural networks

4.1. Neural Networks

Supervised learning requires a labeled dataset, $\{(\mathbf{x}_i, \hat{\mathbf{y}}_i)\}_{i=1, \dots, N}$, where the input data \mathbf{x}_i (features, also called *input feature vector*) are paired with the correct output $\hat{\mathbf{y}}_i$

(labels or target values) the index i iterating over all the N data points (also called *samples*). To perform classification, we employ a feedforward neural network, specifically a multilayer perceptron (MLP), as our machine learning model. An MLP consists of three primary parts: the *input layer*, the *hidden layer(s)*, and the *output layer*. Each layer is composed of neurons, which are the fundamental units of a neural network. In a fully connected neural network, each neuron in a layer receives an input from each neuron of the preceding layer and calculates a real-valued output which is passed on to the next layer.

To illustrate the concept, consider a MLP consisting of $L + 1$ layers (as depicted in Fig. 2), with the input layer identified by the index $l = 0$ and the output layer by the index $l = L$. The value of the $D^{(l)}$ neurons in layer l are calculated from the values of the $D^{(l-1)}$ neurons in layer $l - 1$, with

$$\mathbf{y}^{(l)} = f^{(l)}(\mathbf{z}^{(l)}), \quad (13a)$$

where $f^{(l)}$ is a nonlinear function called the *activation function*, and

$$\mathbf{z}^{(l)} = \mathbf{w}^{(l)}\mathbf{y}^{(l-1)} + \mathbf{b}^{(l)}. \quad (13b)$$

Here $\mathbf{w}^{(l)} \in \mathbb{R}^{D^{(l)} \times D^{(l-1)}}$ is the weight matrix, $\mathbf{b}^{(l)} \in \mathbb{R}^{D^{(l)}}$ is called the *bias vector* and $\mathbf{y}^{(l-1)} \in \mathbb{R}^{D^{(l-1)}}$ are the values of the neurons in layer $l - 1$. The values of the input layer

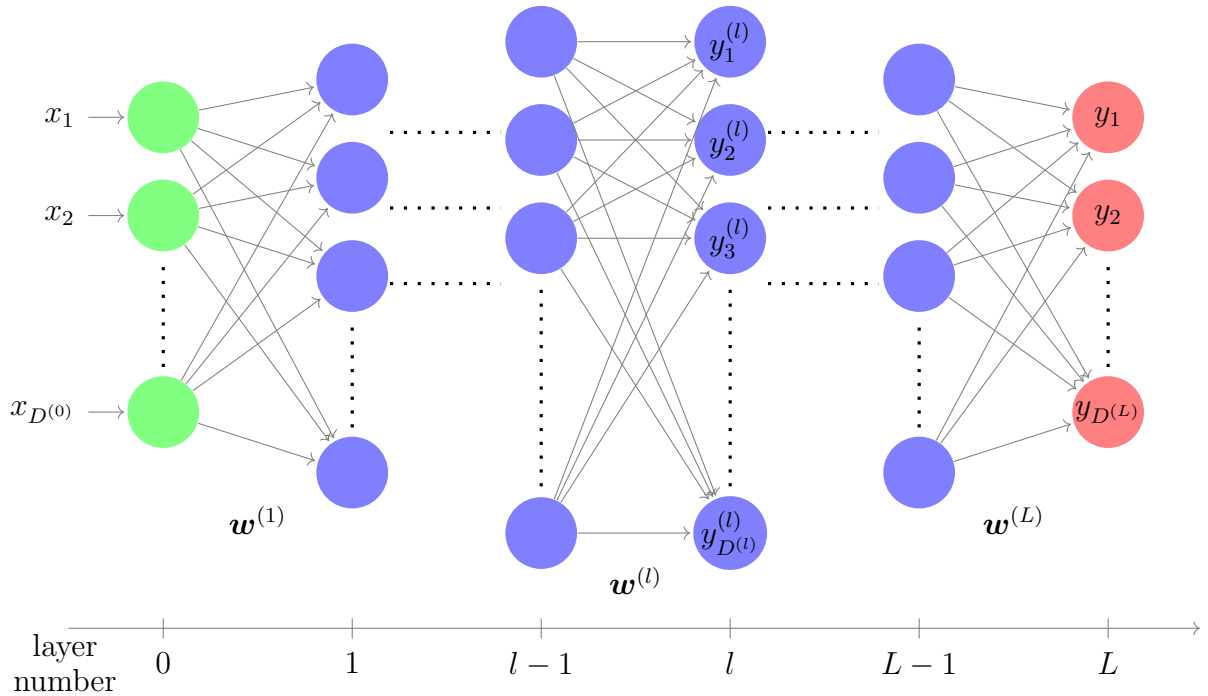


Figure 2. Schematic representation of a Multi Layer Perceptron (MLP) with $L - 1$ hidden layers. $(x_1, x_2, \dots, x_{D^{(0)}})$ are the inputs to the MLP, $\mathbf{w}^{(l)}$ are the weights connecting layer $l - 1$ with layer l and $(y_1, y_2, \dots, y_{D^{(L)}})$ are the outputs. Details on its working are given in the text.

$l = 0$ are set to be the input feature vector $\mathbf{y}^{(0)} = \mathbf{x}$, while the values of the output layer $\mathbf{y}^{(L)}$ is the output that the model associates to the given input: it is called *predicted output* and we indicate it simply as $\mathbf{y} = \mathbf{y}^{(L)}$. The weight matrices, together with the biases and the activation functions, govern the collective influence of the neurons from one layer to the next.

The training process consists in finding weights $\mathbf{W} = \{\mathbf{w}^{(l)}\}_{l=1,2,\dots,L}$ and biases $\mathbf{B} = \{\mathbf{b}^{(l)}\}_{l=1,2,\dots,L}$ such that the model predicts the correct output given an input, and is able to generalize to unseen inputs. This is done by minimizing a cost function $C(\{\mathbf{y}_i, \hat{\mathbf{y}}_i\}_i | \mathbf{W}, \mathbf{B})$ which measures the average distance (“error”) between the NN predicted output \mathbf{y}_i and the target output $\hat{\mathbf{y}}_i$. Typically, this minimization process is executed using algorithms such as *stochastic gradient descent* or its variants. The gradients needed for these optimization algorithms are computed through backpropagation, a highly efficient algorithm that leverages the chain rule to propagate errors backward through the network.

We use a neural network consisting of two hidden layers and the *leaky rectified linear unit* (LeakyReLU) [69] as an activation function for both the hidden layers, for details see Tab. 1. LeakyReLU is defined as

$$f_{\text{LReLU}}(z) = \begin{cases} z & \text{if } z \geq 0, \\ \alpha z & \text{if } z < 0, \end{cases} \quad (14)$$

where α is a constant that we set to the value 0.01. This activation function helps to avoid the “dying ReLU” problem [70], that is problem of obtaining always the same output (often the null one), regardless of the input.

As we are performing a classification task, the output of the NN represents the possible classes (labels). This is accomplished with one-hot encoding: each class is represented by a binary vector with a length $D^{(L)}$ equal to the number of classes, where all elements are zero except for the one corresponding to the specific class, which is set to one. This representation ensures that categorical values are treated as distinct entities by the model, avoiding any implicit ordering that might be inferred from numerical encoding. The output of the network for a given input \mathbf{x}_i is then a vector where each

Layer	# neurons	Activation function
input	3	
hidden 1	128	LeakyReLU
hidden 2	100	LeakyReLU
output	4 or 5	Softmax

Table 1. Structure of the neural network used for classification of the 4 or 5 classes of noise.

element corresponds to the probability that \mathbf{x}_i belongs to one of the possible classes. This is achieved by the use of the *softmax* activation function for the output layer

$$\mathbf{y} = f_{\text{softmax}}(\mathbf{z}^{(L)}) = \frac{e^{\mathbf{z}^{(L)}}}{\sum_{k=1}^{D^{(L)}} e^{z_k^{(L)}}}, \quad (15)$$

which ensures the normalization of \mathbf{y} (the exponentiation is intended to act component-wise). Finally, the class with the highest probability is taken as the model's prediction for the input's class.

We employ the *Categorical cross-entropy* as cost function defined as

$$C(\{\mathbf{y}_i, \hat{\mathbf{y}}_i\}_i) = -\frac{1}{N} \sum_{i=1}^N \sum_{j=1}^{D^{(L)}} \hat{y}_{ij} \ln(y_{ij}), \quad (16)$$

where y_{ij} denotes the components of the predicted output \mathbf{y}_i , i.e. the probability assigned by the model for \mathbf{x}_i to belong to the class $j = 1, \dots, D^{(L)}$ while \hat{y}_{ij} gives the components of the one-hot encoded target vector $\hat{\mathbf{y}}_i$.

4.2. Data generation

In order to efficiently classify between the different noise types it is imperative to identify features which are sensitive to the distinct characteristics of the classes introduced in Sec. 2. To this end, we choose as features the efficiency of the CTAP/STIRAP protocol under three different driving conditions. Referring to Eqs. (7) we consider: (i) $\Omega_p^{\text{max}} = \Omega_s^{\text{max}}$, (ii) $\Omega_p^{\text{max}} > \Omega_s^{\text{max}}$, (iii) $\Omega_p^{\text{max}} < \Omega_s^{\text{max}}$. For each type of noise, we solve numerically the dynamics of the system under the three driving conditions and compute the efficiency as described in Sec. 3. We denote the efficiencies as $\xi_{p=s}$, $\xi_{p>s}$, and $\xi_{p<s}$, for the driving conditions (i), (ii), and (iii) respectively, and we use $\mathbf{x} = (\xi_{p=s}, \xi_{p>s}, \xi_{p<s})$ as input feature vector to the NN, see Fig. 3. The parameters we use are (i) $\Omega_p^{\text{max}} = \Omega_s^{\text{max}} = 50/T$, (ii) $\Omega_p^{\text{max}} = 20\sqrt{10}/T > \Omega_s^{\text{max}} = 10\sqrt{10}/T$, and (iii) $\Omega_p^{\text{max}} = 10\sqrt{10}/T < \Omega_s^{\text{max}} = 20\sqrt{10}/T$ with evolution time $t \in [-5T, 5T]$, $\tau = 0.7T$ and $\sigma_1 \approx 17.6/T$ being the standard deviation of the Gaussian distribution $p_1(x_1, t)$.

For the correlated and anti-correlated noise, data are generated by randomly sampling the correlation parameter η in the intervals $[0.1, 5]$ and $[-5, -0.1]$, respectively. For each randomly selected η we calculate three efficiencies, one for each of the pulse conditions (i), (ii), and (iii), thus generating the input feature vector \mathbf{x} . The efficiencies are calculated using Eq. (10) for non-Markovian quasistatic noise (with $p_1(x_1, t)$ being a Gaussian distribution) and Eq. (12) for Markovian noise.

For uncorrelated, non-Markovian quasistatic noise, the values of \tilde{x}_1 and \tilde{x}_2 are independently sampled from two Gaussian probability distributions $p_1(x_1, t)$ and $p_2(x_2, t)$ with mean $\mu_1 = \mu_2 = 0$. The standard deviation σ_1 of the first distribution is kept fixed, while the standard deviation σ_2 of the distribution $p_2(x_2, t)$ is randomly sampled in the interval $[-5\sigma_1, 5\sigma_1]$. As mentioned in Sec. 4.1, the classes are one-hot

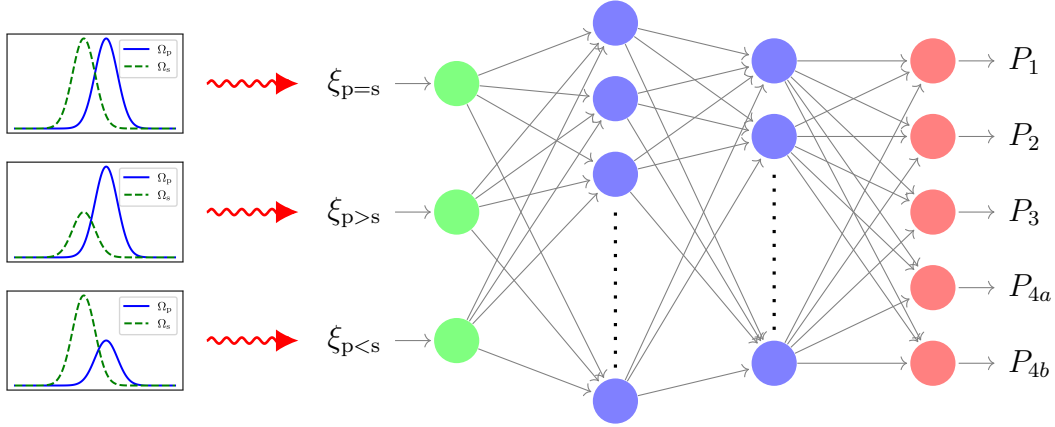


Figure 3. Schematic representation of our model. The efficiencies obtained with the three driving conditions $\Omega_p^{\max} = \Omega_s^{\max}$, $\Omega_p^{\max} > \Omega_s^{\max}$, and $\Omega_p^{\max} < \Omega_s^{\max}$ are given as input to the neural network. The Neural Network is composed of 2 hidden layers with 128 and 100 neurons respectively, and activation function LeakyReLU, Eq. (14). The output layer composed of 4 or 5 neurons represent the probability of assigning each data to the relative noise class. This is achieved with the softmax activation function, Eq. (15), on the output layer.

encoded, thus the output of the neural network is a layer with four or five neurons. For each noise class, we generate 500 samples such that the total data consists of 2000 or 2500 data points $\{\mathbf{x}, \hat{\mathbf{y}}\}$. We then split the data in a training, validation and test set with a ratio of 0.6 : 0.2 : 0.2, respectively.

In order to evaluate the efficacy of the model we use the accuracy A defined as the number of correct predictions divided by the number of total predictions N

$$A = \frac{1}{N} \sum_{i=1}^N \delta(\arg \max \mathbf{y}_i, \arg \max \hat{\mathbf{y}}_i), \quad (17)$$

where the $\arg \max$ function yields the index j of the maximal component of \mathbf{y} and $\delta(\cdot)$ is the Kronecker delta.

5. Results

The ML model and the training are performed with TensorFlow [71] and the results are shown in Fig. 4. The accuracy A for the training and validation sets is shown in Fig. 4(a). After training on the test set the accuracy of the model is $A \approx 0.81$ and varies within the values of approx 0.79 and 0.81 depending on the random initialization of the NN weights and the random shuffling of the data for the splitting in the three sets. For the same test set, we report in Fig. 4(b) how the value of the cost function C changes during training. In Fig. 5, we show the confusion matrix for the trained model, a tabular representation used to evaluate the performance of a classification model. It cross-tabulates the actual class labels with the model's predictions, providing insight into the correct and incorrect classifications made by the model. Thus it helps to

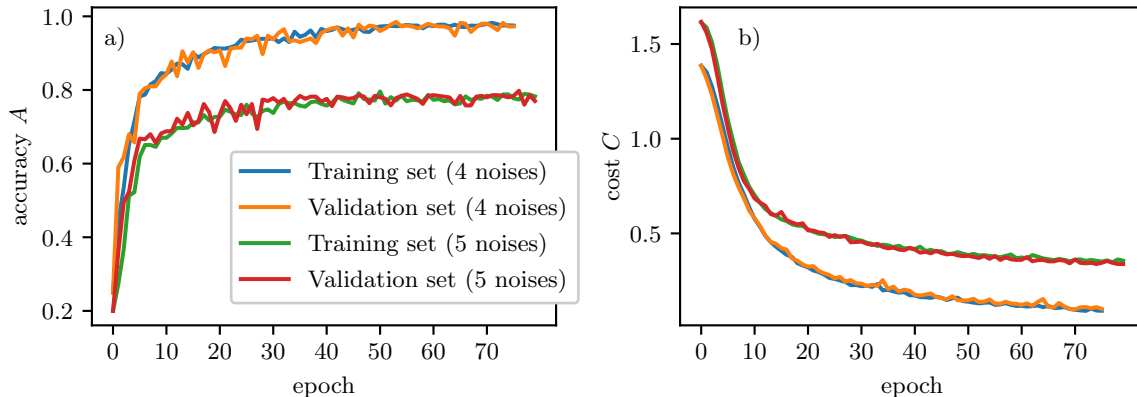


Figure 4. (a) Accuracy, Eq. (17), and (b) value of the cost function, Eq. (16), for the training (blue for four noises and green for five noises) and validation (orange for four noises and red for five noises) sets versus the number of epochs of training. The accuracy on the test set is $A \approx 1$ for four noise classes and $A \approx 0.81$ for five noise classes.

identify which classes are not easily distinguishable from each other posing a challenge to the classification. Each row of the matrix represents the instances of the actual classes, while each column represents the instances of the predicted classes. It is apparent from Fig. 5(a) that classes $4a$ and $4b$ are not distinguishable from each other with the input features of our choice and almost all the samples collapse in class $4a$.

We then repeat the same analysis considering the Markovian noise as a single class, i.e. by grouping together correlated and anti-correlated noise and taking $\eta \in [-5, 5]$. As expected, the effectiveness of the model increases reaching an accuracy $A \approx 1$ that varies between $\simeq 0.97$ and 1 depending on the random initialization. The accuracy A and the value of the cost function C during the training are shown in Fig. 4. The confusion matrix for this model is reported in Fig. 5(b) showing that now the four classes are clearly distinguishable with the chosen input features.

5.1. Results for a finite number of measurement

The analysis performed in the previous section describes the ideal physical situation that the data are obtained from an infinite number of 100%-efficiency of projective quantum measurements. While very large efficiency can be achieved by quantum non-demolition measurements [72], in this section we analyze how the training and the accuracy of the model are affected by the number of measurements M being finite. To this end, we employ the same method described in Sec. 4.2 but compute the efficiency ξ_M as the one resulting from a set of individual “quantum” trajectories. The result of unravelling each trajectory is simulated by extracting each time the value 1 with probability equal to the population of the target state $|2\rangle$. The output \mathbf{y} is produced by averaging over the M quantum trajectories. We produce 500 distinct datasets, each corresponding

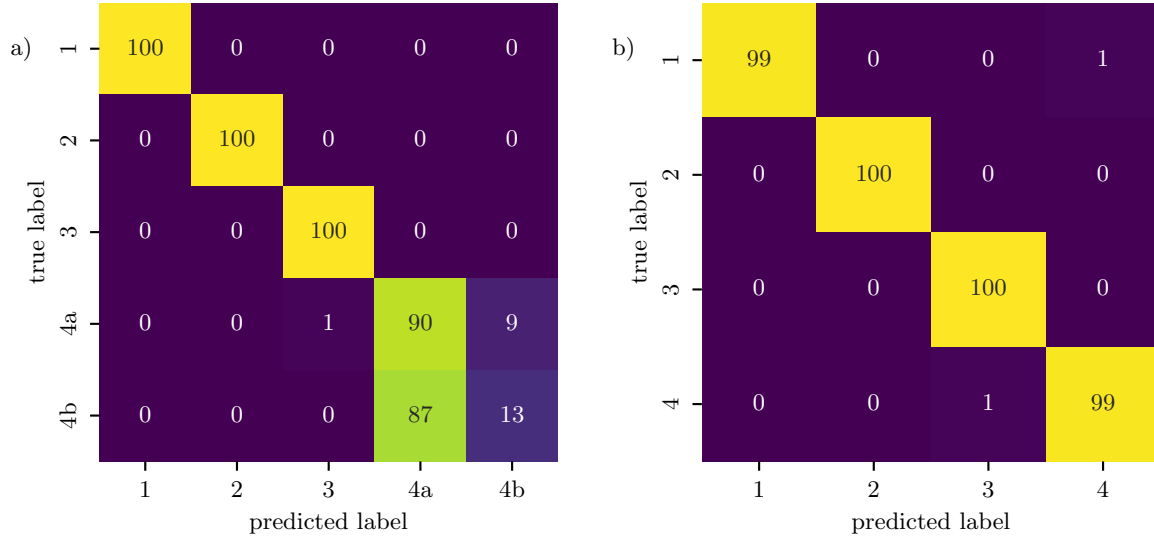


Figure 5. Confusion matrix for the MLP model for the classification of the classes of noise considered in this work. Each row of the matrix represents the instances of the true classes, while each column represents the instances of the predicted classes. It is apparent that classes 4a and 4b, i.e. Markovian correlated and anti-correlated, are not easily distinguishable.

to a different measurement count $M = 10, \dots, 5000$ (in steps of 10). For each M , we train the model and evaluate its accuracy using the same methodology as previously described.

The results are presented in Fig. 6, where we report the accuracy versus the number of measurements. As expected, the accuracy improves for increasing M , approaching the value obtained in the ideal case, which lies in the range $A \approx [0.97, 1]$.

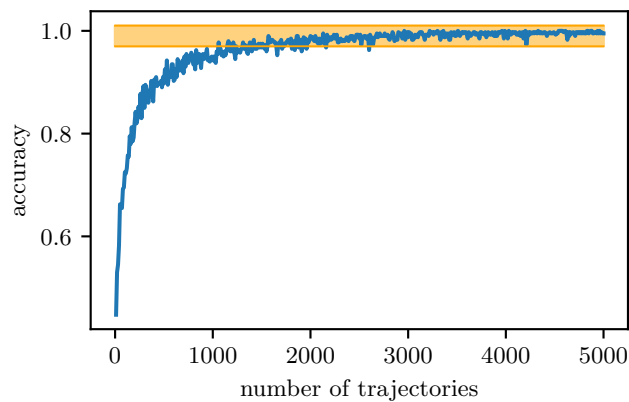


Figure 6. Accuracy of the classification task for four classes of noise versus the number M of projective measurements on quantum trajectories. The shaded orange region corresponds to the accuracy obtained with ideal measurements.

6. Physical implementation and interpretation of the results

6.1. Physical implementations of the model

Spatially correlated noise in solid-state quantum information processing is a topic of current experimental investigation in superconducting [51] and semiconducting [53] quantum devices. Hardware CTAP has been demonstrated in arrays of quantum dots [73]. In superconducting devices STIRAP has been demonstrated in Vee configuration [74–76] whereas the Lambda configuration we study in this work could be implemented either directly [77–79] or by a detuning-modulated protocol [80] generalizing hyper-STIRAP [60] which bypasses parity selection rules enforced at noise-protected operating points.

Diagonal noise such as the one addressed here describes the effect of sources producing a fluctuating electrical polarization of charges. In principle, noise and correlations may also affect the tunneling amplitudes, thus giving rise to fluctuations of the non-diagonal entries of the Hamiltonian. However, as long as the noise is smaller than (δ, δ_p) , as in our case, off-diagonal noise affects the dynamics only at second order and gives rise to a higher-order effect that can be neglected. For STIRAP in multilevel artificial atoms, noise correlations stem due to the fact that each noise source is coupled to the device via a single operator. In particular, noise coupled by an operator commuting with the undriven Hamiltonian (referred as “longitudinal”) yields stochastic fluctuations of the energy splittings of the devices which are related to each other. The main effect is diagonal noise, the off-diagonal entries being negligible if noise is smaller than the Autler-Townes splitting $\propto \sqrt{\Omega_p^2 + \Omega_s^2}$ (see Appendix B). Notice that in this case, the parameter η is fully determined by the first derivatives of the band structure at the point where the device is biased.

6.2. Interpretation of the results

We now seek an explanation of the ability to classify among differently correlated non-Markovian quasistatic noises. To this end, we analyze the stability plots (efficiency versus the detunings δ and δ_p) for the three driving conditions, shown in Fig. 7

Ideally, the system is operated at zero detunings, $\delta = \delta_p = 0$. The effect of quasistatic noise is to move, at each individual repetition of the protocol, the point associated with the operations of the system to somewhere else in the space of parameters [cf. Fig.7]. The efficiency for correlated and anti-correlated noise types, is calculated as a weighed average over the line $\delta = \eta\delta_p$, see Eq. (10). The corresponding efficiency depends on the ratio between Ω_p^{\max} and Ω_s^{\max} , this dependence being different for $\eta > 0$ or $\eta < 0$. Fig. 7 reports as an example the lines $\delta = \eta\delta_p$ for $\eta \geq 0$: it is clear that for $\eta > 0$ the efficiency of CTAP with $\Omega_p^{\max} < \Omega_s^{\max}$ is higher than the one with $\Omega_p^{\max} > \Omega_s^{\max}$, and vice versa for $\eta < 0$. For a more extensive analysis of this behavior we refer to Ref. [81]. For uncorrelated noise, instead, the average is over the whole $\delta - \delta_p$ plane – cf. Eq. (9) – and its dependence on the three different driving conditions is not as explicit.

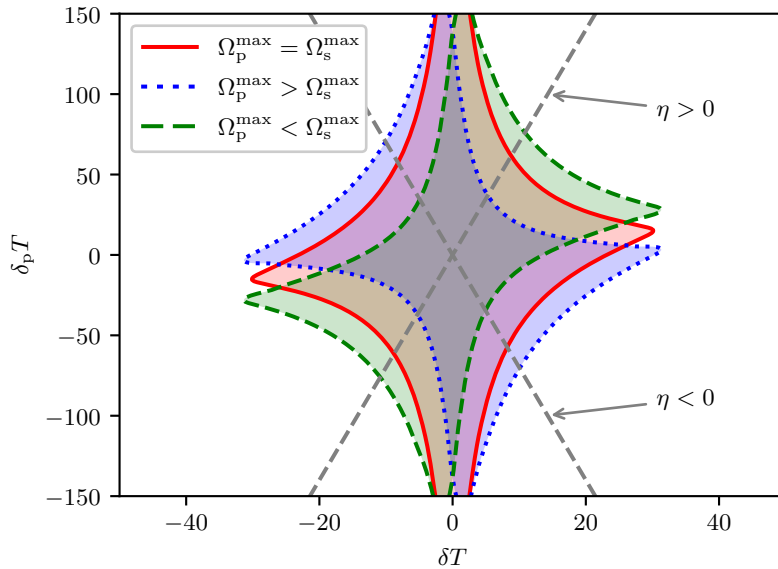


Figure 7. Efficiency of CTAP for the three driving conditions (i) $\Omega_p^{\max} = \Omega_s^{\max} = 50/T$ (red, solid line), (ii) $\Omega_p^{\max} = 20\sqrt{10}/T > \Omega_s^{\max} = 10\sqrt{10}/T$ (blue, dotted line), and (iii) $\Omega_p^{\max} = 10\sqrt{10}/T < \Omega_s^{\max} = 20\sqrt{10}/T$ (green dashed line). The shaded areas within the boundary lines highlight the regions, in the parameter space, where the efficiency is > 0.7 (the efficiency being exactly 0.7 along the boundary curves). The efficiencies are calculated with Eqs. (9) and (10). The dashed gray lines represent correlation ($\eta > 0$) or anti-correlation ($\eta < 0$) between the detunings δ and δ_p . The other parameter is $\tau = 0.7T$.

Such analysis cannot be replicated for Markovian noise, as individual trajectories cannot be represented as single points in Fig. 7. Instead, the noise assumes all values along the line $\delta = \eta\delta_p$ during each repetition of the protocol.

7. Conclusions

We have proposed a ML-based method for categorizing correlated classical noise affecting a three-level quantum system. We have considered various instances of non-Markovian and Markovian noise, including(anti-)correlated and uncorrelated mechanisms.

We have shown that exploiting the sensitivity of a CTAP/STIRAP protocol to correlation and Markovianity, it is possible to successfully classify with great detail the noise mechanisms. Specifically, the efficiency of population transfer under three different driving conditions is sufficient to distinguish among the correlations of non-Markovian quasistatic noise, and between the latter and Markovian noise. On the contrary, this approach is inadequate to differentiate between the correlations in Markovian noise. As input to the ML analysis, we have used the solution of the Stochastic Schrödinger equation and the Markovian Lindblad Master Equation which yield the result of averaging over an infinite number of projective quantum measurements. Our study has been complemented by the analysis of the impact of statistical measurement errors,

showing that our approach is robust against those arising from finite statistics.

We remark that the implications of our work extend beyond noise classification. The methodology developed herein offers a novel perspective on the use of quantum protocols, such as CTAP/STIRAP and their multilevel/multiqubit extensions, not just for quantum control but also as diagnostic tools for system-characterization.

Future directions of this research include investigating the potential of incorporating alternative features of the input and extending this approach to other classes of noise, and the use of unsupervised learning. Additionally, we aim to address the interplay with relaxation [78, 82] and explore the application of this approach to more complex quantum structures, such as interacting multiqubit systems [61] as well as strongly [83] and ultrastrongly coupled [84, 85] architectures exploiting new STIRAP protocols controlled by detunings [9, 86]. This work and the foreseen advances could provide important elements for the development of integrated robust quantum control and error correction techniques.

Acknowledgments

The authors acknowledge Dario Allegra, Lorenzo Catania, Vincenzo Minissale and Giuliano Chiriacò for useful discussions. SM acknowledges support from the project PON Ricerca e Innovazione 2014-2020, React EU, Axis IV, Action IV.4 (CUP: E69J21011430006), within the PhD course in Physics of the Catania University. LG and EP acknowledge support from the PNRR MUR project PE0000023-NQSTI; GF is supported by the ICSC – Centro Nazionale di Ricerca in High-Performance Computing, Big Data and Quantum Computing. GF and EP acknowledge support from the University of Catania, Piano Incentivi Ricerca di Ateneo 2020-22, project Q-ICT. EP acknowledges the COST Action SUPERQUMAP (CA 21144). MP acknowledges support from the European Union’s Horizon Europe EIC-Pathfinder project QuCoM (grant no. 101046973), the Royal Society Wolfson Fellowship (grant no. RSWF/R3/183013), the UK EPSRC (grant no. EP/T028424/1), and the Department for the Economy Northern Ireland under the US-Ireland R&D Partnership Programme.

Appendix A. Derivation of the Lindblad master equation for Markovian diagonal classical noise

Here we derive the Lindblad master equation introduced in Eq. (11) for the description of the dynamics of the system when it is subject to Markovian noise. As mentioned in Sec. 2, the total Hamiltonian of the system is $H = H_{\text{sys}} + H_{\text{noise}}$, where H_{noise} is given by Eq. (2). Using the correlation $x_2(t) = \eta x_1(t)$, we can represent H_{noise} as

$$H_{\text{noise}} = \tilde{x}_1(t) (|1\rangle\langle 1| + \eta|2\rangle\langle 2|) = \tilde{x}_1(t)O, \quad (\text{A.1})$$

where $O = |1\rangle\langle 1| + \eta|2\rangle\langle 2|$ is the noise operator. For Markovian noise, the noise has zero mean $\langle \tilde{x}_1(t) \rangle = 0$ and is delta-correlated as $\langle \tilde{x}_1(t)\tilde{x}_1(t') \rangle = \hbar^2\gamma\delta(t-t')$. Since the noise is δ correlated, the variation of the tunneling amplitudes $\Omega_p(t)$ and $\Omega_s(t)$ is adiabatic, thus we consider an instantaneous interaction picture

$$\tilde{\rho}(t) = e^{\frac{i}{\hbar}H_{\text{sys}}t}\rho(t)e^{-\frac{i}{\hbar}H_{\text{sys}}t}, \quad (\text{A.2})$$

where $\rho(t)$ is the density operator in the Schrödinger picture. The time evolution of the system is thus given by

$$\dot{\tilde{\rho}}(t) = -\frac{i}{\hbar}[\tilde{H}_{\text{noise}}(t), \tilde{\rho}(t)], \quad (\text{A.3})$$

with $\tilde{H}_{\text{noise}}(t) = e^{\frac{i}{\hbar}H_{\text{sys}}t}H_{\text{noise}}(t)e^{-\frac{i}{\hbar}H_{\text{sys}}t}$. Integrating the above equation within the time limits $[0, t]$, we get

$$\tilde{\rho}(t) = \tilde{\rho}(0) - \frac{i}{\hbar} \int_0^t [\tilde{H}_{\text{noise}}(t'), \tilde{\rho}(t')] dt'. \quad (\text{A.4})$$

Substituting $\tilde{\rho}(t)$ in Eq. (A.3) we obtain

$$\dot{\tilde{\rho}}(t) = -\frac{i}{\hbar}e^{\frac{i}{\hbar}H_{\text{sys}}t}[\tilde{x}_1(t)O\rho(0) - \rho(0)O\tilde{x}_1(t)]e^{-\frac{i}{\hbar}H_{\text{sys}}t} - \frac{1}{\hbar^2} \int_0^t [\tilde{H}_{\text{noise}}(t), [H_{\text{noise}}(t'), \tilde{\rho}(t')]] dt'. \quad (\text{A.5})$$

Averaging over the stochastic variable at time t , we obtain

$$\langle \dot{\tilde{\rho}}(t) \rangle = -\frac{1}{\hbar^2} \left\langle \int_0^t [\tilde{x}(t)\tilde{O}(t), [\tilde{x}(t')\tilde{O}(t'), \tilde{\rho}(t')]] dt' \right\rangle, \quad (\text{A.6})$$

where, $\tilde{O}(t) = e^{\frac{i}{\hbar}H_{\text{sys}}t}Oe^{-\frac{i}{\hbar}H_{\text{sys}}t}$. Taking into account that $t' < t$ and $\tilde{\rho}(t')$ cannot depend on t except for $t' = t$, we can write $\langle \tilde{x}(t)\tilde{x}(t')\tilde{\rho}(t') \rangle = \langle \tilde{x}(t)\tilde{x}(t') \rangle \tilde{\rho}(t')$. We thus obtain

$$\langle \dot{\tilde{\rho}}(t) \rangle = -\frac{\gamma}{2} \left(\tilde{O}^2(t)\tilde{\rho}(t) + \tilde{\rho}(t)\tilde{O}^2(t) - 2\tilde{O}(t)\tilde{\rho}(t)\tilde{O}(t) \right). \quad (\text{A.7})$$

Finally, the above equation in the Schrödinger picture can be represented in the Lindblad form as

$$\langle \dot{\rho}(t) \rangle = -\frac{i}{\hbar}[H_{\text{sys}}, \rho(t)] - \frac{\gamma}{2} (O^2(t)\rho(t) + \rho(t)O^2(t) - 2O(t)\rho(t)O(t)). \quad (\text{A.8})$$

Appendix B. Adiabatic passage in a three-node network

Recall the Hamiltonian of the three-node network $H_{\text{sys}}(t) = H_0 + H_c(t)$, where H_0 and $H_c(t)$ are the uncoupled and the control parts, respectively ($\hbar = 1$):

$$H_0 = \delta_p |1\rangle\langle 1| + \delta |2\rangle\langle 2|, \quad (\text{B.1a})$$

$$H_c = \frac{\Omega_p(t)}{2} (|0\rangle\langle 1| + |1\rangle\langle 0|) + \frac{\Omega_s(t)}{2} (|1\rangle\langle 2| + |2\rangle\langle 1|), \quad (\text{B.1b})$$

where $\delta_p = \epsilon_1 - \epsilon_0$ and $\delta = \epsilon_2 - \epsilon_0$ define the detunings. CTAP (Coherent Tunneling by Adiabatic Passage) [56] (as well as its spin equivalent spin-CTAP [64]) is a protocol that achieves population transfer from $|0\rangle$ to $|2\rangle$ without populating the state $|1\rangle$ by adiabatic following a trapped state. The atomic analogue is called STIRAP [60, 63] where high-fidelity population transfer occurs via a dark state. These protocols have remarkable robustness against parametric fluctuations.

The CTAP protocol is based on the counter-intuitive ordering of the pulses $\Omega_p(t)$ and $\Omega_s(t)$ and the condition $\delta \approx 0$ is essential for the successful population transfer [63]. Considering thus $\delta = 0$, the instantaneous eigenstates of $H_{\text{sys}}(t)$, are

$$|\phi_D(t)\rangle = \cos \theta(t) |0\rangle - \sin \theta(t) |2\rangle, \quad (\text{B.2a})$$

$$|\phi_-(t)\rangle = \sin \theta(t) \cos \phi(t) |0\rangle - \sin \phi(t) |1\rangle + \cos \theta(t) \cos \phi(t) |2\rangle, \quad (\text{B.2b})$$

$$|\phi_+(t)\rangle = \sin \theta(t) \sin \phi(t) |0\rangle - \cos \phi(t) |1\rangle + \cos \theta(t) \sin \phi(t) |2\rangle, \quad (\text{B.2c})$$

with corresponding eigenvalues

$$\lambda_D(t) = 0, \quad (\text{B.3a})$$

$$\lambda_-(t) = -\frac{\hbar}{2} \sqrt{\Omega_p(t)^2 + \Omega_s(t)^2} \tan \phi(t), \quad (\text{B.3b})$$

$$\lambda_+(t) = \frac{\hbar}{2} \sqrt{\Omega_p(t)^2 + \Omega_s(t)^2} \cot \phi(t), \quad (\text{B.3c})$$

where

$$\theta(t) = \tan^{-1} \left(\frac{\Omega_p(t)}{\Omega_s(t)} \right), \quad (\text{B.4})$$

$$\phi(t) = \tan^{-1} \left(\frac{\sqrt{\Omega_p(t)^2 + \Omega_s(t)^2}}{\delta_p + \sqrt{\delta_p^2 + \Omega_p(t)^2 + \Omega_s(t)^2}} \right). \quad (\text{B.5})$$

The eigenstate $|\phi_D(t)\rangle$ corresponding to zero eigenvalue is called the *trapped state* (or also *dark state*) since it is trapped in the subspace $\{|0\rangle, |2\rangle\}$ (and, in the case of an atom, cannot absorb or emit photons). It has no component along the state $|1\rangle$ and it is the state that the system follows during the population transfer [10]. The states $|\phi_-(t)\rangle$ and $|\phi_+(t)\rangle$ are the Autler-Townes states and $|\lambda_+ - \lambda_-|$ the Autler-Townes splitting.

If the pulses are counter-intuitively ordered, i.e. if Ω_s is applied before Ω_p :

$$\lim_{t \rightarrow t_i} \frac{\Omega_p(t)}{\Omega_s(t)} = \lim_{t \rightarrow t_f} \frac{\Omega_s(t)}{\Omega_p(t)} = 0, \quad (\text{B.6})$$

then the dark state $\phi_D(t)$ at the initial time t_i will coincide with the initial state $|0\rangle$ and at the final time t_f will coincide with the target state $|2\rangle$. If the evolution is adiabatic and the system is initially prepared in $|0\rangle = |\phi_D(t_i)\rangle$, by the adiabatic theorem [65, 66], the system evolves following the dark state $|\phi_D(t)\rangle$ throughout the time evolution. Thus, the population is transferred from state $|0\rangle$ to state $|2\rangle$ never populating the intermediate state $|1\rangle$. The adiabaticity condition for this protocol is given by [56, 60]

$$\hbar|\langle\phi_{\pm}|\dot{\phi}_D\rangle| \ll |\lambda_0 - \lambda_{\pm}|. \quad (\text{B.7})$$

Using the expressions for the dressed bases, Eqs. (B.2) and Eqs. (B.3), in equation (B.7) we have the condition for adiabatic evolution in terms of the pulses [10, 60, 63]

$$|\dot{\theta}(t)| \ll \frac{1}{2} \left| \delta_p \pm \sqrt{\delta_p^2 + \Omega_p(t)^2 + \Omega_s(t)^2} \right|, \quad (\text{B.8})$$

which is called ‘‘local adiabaticity condition’’ and has to hold for all times $t \in [t_i, t_f]$. By time averaging Eq. (B.8) over τ and assuming $\delta_p \ll \Omega_p^{\max}, \Omega_s^{\max}$ one can obtain the less strict ‘‘global adiabaticity condition’’ which is often reported as [60]

$$\Omega_{p/s}^{\max} \tau \geq 10, \quad (\text{B.9})$$

where τ is the characteristic time scale of the pulses overlap and $\Omega_{p/s}^{\max} = \max_t \Omega_{p/s}(t)$.

In this work, in order to perform the population transfer, we use Gaussian pulses of the form

$$\Omega_p(t) = \Omega_p^{\max} e^{-\left(\frac{t-\tau}{T}\right)^2}, \quad (\text{B.10a})$$

$$\Omega_s(t) = \Omega_s^{\max} e^{-\left(\frac{t+\tau}{T}\right)^2}, \quad (\text{B.10b})$$

and we let the system evolve in the time interval $t \in [-5T, 5T]$ with $\tau = 0.7T$, see Fig. 1 for an example of pulses.

We point out that our aim is not achieving an efficient population transfer, but to exploit CTAP to get information about the noise affecting the system and deteriorating the efficiency.

References

- [1] Christiane P. Koch et al. “Quantum Optimal Control in Quantum Technologies. Strategic Report on Current Status, Visions and Goals for Research in Europe”. In: *EPJ Quantum Technol.* 9.1 (2022-12), p. 19.
- [2] Antonio Acín et al. “The Quantum Technologies Roadmap: A European Community View”. In: *New J. Phys.* 20.8 (2018-08), p. 080201.
- [3] Wojciech Hubert Zurek. “Decoherence, Einselection, and the Quantum Origins of the Classical”. In: *Rev. Mod. Phys.* 75.3 (2003-05), pp. 715–775.
- [4] W. G. Unruh. “Maintaining Coherence in Quantum Computers”. In: *Phys. Rev. A* 51.2 (1995-02), pp. 992–997.
- [5] I. L. Chuang et al. “Quantum Computers, Factoring, and Decoherence”. In: *Science* 270.5242 (1995-12), pp. 1633–1635.
- [6] Florian Marquardt. “Machine Learning and Quantum Devices”. In: *SciPost Physics Lecture Notes* (2021-05), p. 029.
- [7] Mario Krenn et al. “Artificial Intelligence and Machine Learning for Quantum Technologies”. In: *Phys. Rev. A* 107.1 (2023-01), p. 010101.
- [8] Valentin Gebhart et al. “Learning Quantum Systems”. In: *Nat Rev Phys* (2023-02), pp. 1–16.
- [9] J. Brown et al. “Reinforcement Learning-Enhanced Protocols for Coherent Population-Transfer in Three-Level Quantum Systems”. In: *New J. Phys.* 23.9 (2021-09), p. 093035.
- [10] Luigi Giannelli et al. “A Tutorial on Optimal Control and Reinforcement Learning Methods for Quantum Technologies”. In: *Physics Letters A* 434 (2022-05), p. 128054.
- [11] Murphy Yuezhen Niu et al. “Universal Quantum Control through Deep Reinforcement Learning”. In: *npj Quantum Inf* 5.1 (2019-04), pp. 1–8.
- [12] Pierpaolo Sgroi, G. Massimo Palma, and Mauro Paternostro. “Reinforcement Learning Approach to Nonequilibrium Quantum Thermodynamics”. In: *Physical Review Letters* 126.2 (2021), p. 020601.
- [13] L. Banchi et al. “Modelling Non-Markovian Quantum Processes with Recurrent Neural Networks”. In: *New J. Phys.* 20.12 (2018-12), p. 123030.
- [14] Giacomo Torlai et al. “Neural-Network Quantum State Tomography”. In: *Nature Phys.* 14.5 (2018-05), pp. 447–450.
- [15] Adriano Macarone Palmieri et al. “Experimental Neural Network Enhanced Quantum Tomography”. In: *npj Quantum Inf* 6.1 (2020-02), pp. 1–5.
- [16] Raphaël Couturier et al. “Characterization of a Driven Two-Level Quantum System by Supervised Learning”. In: *Entropy* 25.3 (2023-03), p. 446.
- [17] Élie Genois et al. “Quantum-Tailored Machine-Learning Characterization of a Superconducting Qubit”. In: *PRX Quantum* 2.4 (2021-12), p. 040355.

- [18] Akram Youssry, Gerardo A. Paz-Silva, and Christopher Ferrie. “Characterization and Control of Open Quantum Systems beyond Quantum Noise Spectroscopy”. In: *npj Quantum Inf.* 6.1 (2020-12), p. 95.
- [19] S. Bandyopadhyay et al. “Applications of Neural Networks to the Simulation of Dynamics of Open Quantum Systems”. In: *Chemical Physics. Ultrafast Photoinduced Processes in Polyatomic Molecules: Electronic Structure, Dynamics and Spectroscopy (Dedicated to Wolfgang Domcke on the Occasion of His 70th Birthday)* 515 (2018-11), pp. 272–278.
- [20] Di Luo et al. “Autoregressive Neural Network for Simulating Open Quantum Systems via a Probabilistic Formulation”. In: *Phys. Rev. Lett.* 128.9 (2022-02), p. 090501.
- [21] I. A. Luchnikov et al. “Machine Learning Non-Markovian Quantum Dynamics”. In: *Phys. Rev. Lett.* 124.14 (2020-04), p. 140502.
- [22] Felipe F. Fanchini et al. “Estimating the Degree of Non-Markovianity Using Machine Learning”. In: *Phys. Rev. A* 103.2 (2021-02), p. 022425.
- [23] Miha Papič and Inés de Vega. “Neural-Network-Based Qubit-Environment Characterization”. In: *Phys. Rev. A* 105.2 (2022-02), p. 022605.
- [24] David F. Wise, John J.L. Morton, and Siddharth Dhomkar. “Using Deep Learning to Understand and Mitigate the Qubit Noise Environment”. In: *PRX Quantum* 2.1 (2021-01), p. 010316.
- [25] J. Barr et al. “Spectral Density Classification for Environment Spectroscopy”. In: *Mach. Learn.: Sci. Technol.* 5.1 (2024-03), p. 015043.
- [26] Stefano M. et al. “Learning the Noise Fingerprint of Quantum Devices”. In: *arXiv:2109.11405 [quant-ph]* (2021-09).
- [27] Stefano Martina et al. “Deep Learning Enhanced Noise Spectroscopy of a Spin Qubit Environment”. In: *Mach. Learn.: Sci. Technol.* 4.2 (2023-05), 02LT01.
- [28] E. Paladino et al. “1/F Noise: Implications for Solid-State Quantum Information”. In: *Rev. Mod. Phys.* 86.2 (2014-04), pp. 361–418.
- [29] D. Vion et al. “Manipulating the Quantum State of an Electrical Circuit”. In: *Science* 296.5569 (2002-05), pp. 886–889.
- [30] A. Ajoy, G. A. Álvarez, and D. Suter. “Optimal Pulse Spacing for Dynamical Decoupling in the Presence of a Purely Dephasing Spin Bath”. In: *Phys. Rev. A* 83.3 (2011-03), p. 032303.
- [31] J. Roffe. “Quantum error correction: an introductory guide”. In: *Contemporary Physics* 60 (2019), p. 226.
- [32] E. Campbell. “A series of fast-paced advances in Quantum Error Correction”. In: *Nat. Rev. Phys.* 6 (2024), p. 160.
- [33] Lorenza Viola, Emanuel Knill, and Seth Lloyd. “Dynamical Decoupling of Open Quantum Systems”. In: *Phys. Rev. Lett.* 82.12 (1999-03), pp. 2417–2421.

- [34] G. Falci et al. “Dynamical suppression of telegraph and $1/f$ noise due to quantum bistable fluctuators”. In: *Phys. Rev. A* 70.4 (2004-10). Publisher: American Physical Society, p. 040101.
- [35] Antonio D’Arrigo et al. *Open-Loop Quantum Control of Small-Size Networks for High-Order Cumulants and Cross-Correlations Sensing*. 2024-01.
- [36] Giuseppe Falci, Pertti J. Hakonen, and Elisabetta Paladino. “ $1/f$ noise in quantum nanoscience”. In: *Encyclopedia of Condensed Matter Physics (Second Edition)*. Ed. by Tapash Chakraborty. Oxford: Academic Press, 2024-01, pp. 1003–1017.
- [37] Alexander A. Balandin, Elisabetta Paladino, and Pertti J. Hakonen. “Electronic noise—From advanced materials to quantum technologies”. In: *Applied Physics Letters* 124.5 (2024-01), p. 050401.
- [38] Francesco M. D. Pellegrino, Giuseppe Falci, and Elisabetta Paladino. “ $1/f$ critical current noise in short ballistic graphene Josephson junctions”. en. In: *Commun Phys* 3.1 (2020-01). Publisher: Nature Publishing Group, pp. 1–8.
- [39] Michael J. Biercuk et al. “Optimized dynamical decoupling in a model quantum memory”. In: *Nature* 458 (2009), p. 996.
- [40] Michael J. Biercuk et al. “Experimental Uhrig dynamical decoupling using trapped ions”. In: *Phys. Rev. A* 79 (2009), p. 062324.
- [41] S. Damodarapur et al. “Experimental Inhibition of Decoherence on Flying Qubits via “Bang-Bang” Control”. In: *Phys. Rev. Lett.* 103 (4 2009-07), p. 040502.
- [42] Gonzalo A. Álvarez et al. “Performance comparison of dynamical decoupling sequences for a qubit in a rapidly fluctuating spin bath”. In: *Phys. Rev. A* 82 (2010), p. 042306.
- [43] E. R. Jenista et al. “Optimized, unequal pulse spacing in multiple echo sequences improves refocusing in magnetic resonance”. In: *J. Chem. Phys.* 131 (2009), p. 204510.
- [44] Boris Naydenov et al. “Dynamical decoupling of a single-electron spin at room temperature”. In: *Phys. Rev. B* 83 (8 2011-02), p. 081201.
- [45] J.-M. Cai et al. “Robust dynamical decoupling with concatenated continuous driving”. In: *New J. Phys.* 14 (2012), p. 113023.
- [46] Morten Kjaergaard et al. “Superconducting Qubits: Current State of Play”. en. In: *Annu. Rev. Condens. Matter Phys.* 11.1 (2020-03), pp. 369–395.
- [47] Youngkyu Sung et al. “Multi-level quantum noise spectroscopy”. en. In: *Nat Commun* 12.1 (2021-02). Publisher: Nature Publishing Group, p. 967.
- [48] A. D’Arrigo et al. “Effects of low-frequency noise cross-correlations in coupled superconducting qubits”. en. In: *New J. Phys.* 10.11 (2008-11), p. 115006.
- [49] Antti P. Vepsäläinen et al. “Impact of ionizing radiation on superconducting qubit coherence”. en. In: *Nature* 584.7822 (2020-08). Publisher: Nature Publishing Group, pp. 551–556.

- [50] A. B. Zorin et al. “Background Charge Noise in Metallic Single-Electron Tunneling Devices”. In: *Phys. Rev. B* 53.20 (1996-05), pp. 13682–13687.
- [51] Uwe von Lüpke et al. “Two-Qubit Spectroscopy of Spatiotemporally Correlated Quantum Noise in Superconducting Qubits”. In: *PRX Quantum* 1.1 (2020-09). Publisher: American Physical Society, p. 010305.
- [52] J. Yoneda et al. “Noise-correlation spectrum for a pair of spin qubits in silicon”. en. In: *Nat. Phys.* 19.12 (2023-12). Number: 12 Publisher: Nature Publishing Group, pp. 1793–1798.
- [53] Ji Zou, Stefano Bosco, and Daniel Loss. *Spatially correlated classical and quantum noise in driven qubits: The good, the bad, and the ugly*. arXiv:2308.03054 [cond-mat, physics:quant-ph]. 2023-08.
- [54] G. Chiriaco et al. “Diagrammatic Method for Many-Body Non-Markovian Dynamics: Memory Effects and Entanglement Transitions”. In: *Phys. Rev. B* 108.7 (2023-08), p. 075151.
- [55] Mikheil Tsitsishvili et al. “Measurement induced transitions in non-Markovian free fermion ladders”. In: *SciPost Phys. Core* 7 (2024), p. 011.
- [56] Andrew D. Greentree et al. “Coherent Electronic Transfer in Quantum Dot Systems Using Adiabatic Passage”. In: *Phys. Rev. B* 70.23 (2004-12), p. 235317.
- [57] A. Burkov. *The Hundred-Page Machine Learning Book*. Vol. 1. Andriy Burkov Quebec City, QC, Canada, 2019.
- [58] Aurélien Géron. *Hands-on Machine Learning with Scikit-Learn, Keras, and TensorFlow: Concepts, Tools, and Techniques to Build Intelligent Systems*. Third edition. Beijing Boston Farnham Sebastopol Tokyo: O’Reilly, 2023.
- [59] Ian Goodfellow, Yoshua Bengio, and Aaron Courville. *Deep Learning*. Adaptive Computation and Machine Learning. Cambridge, Massachusetts: The MIT Press, 2016.
- [60] K. Bergmann, H. Theuer, and B. W. Shore. “Coherent Population Transfer among Quantum States of Atoms and Molecules”. In: *Rev. Mod. Phys.* 70.3 (1998-07), pp. 1003–1025.
- [61] J. Yoneda et al. “Noise-Correlation Spectrum for a Pair of Spin Qubits in Silicon”. In: *Nat. Phys.* (2023-10), pp. 1–6.
- [62] Leonard Mandel and Emil Wolf. *Optical Coherence and Quantum Optics*. Cambridge ; New York: Cambridge University Press, 1995.
- [63] Nikolay V Vitanov et al. “Stimulated Raman Adiabatic Passage in Physics, Chemistry, and Beyond”. In: *Reviews of Modern Physics* 89.1 (2017), p. 015006.
- [64] M. J. Gullans and J. R. Petta. “Coherent Transport of Spin by Adiabatic Passage in Quantum Dot Arrays”. In: *Phys. Rev. B* 102.15 (2020-10), p. 155404.
- [65] M. Born and V. Fock. “Beweis Des Adiabatenatzes”. In: *Zeitschrift für Physik* 51.3-4 (1928), pp. 165–180.

- [66] A. Messiah. *Quantum Mechanics, Vol. 1/2*. North-Holland, Amsterdam, 1961.
- [67] Luigi Giannelli and Ennio Arimondo. “Three-Level Superadiabatic Quantum Driving”. In: *Phys. Rev. A* 89.3 (2014-03), p. 033419.
- [68] Crispin W. Gardiner and Peter Zoller. *Quantum Noise: A Handbook of Markovian and Non-Markovian Quantum Stochastic Methods with Applications to Quantum Optics*. 3. ed., [Nachdr.] Springer Series in Synergetics. Berlin Heidelberg: Springer, 2010.
- [69] Andrew L Maas, Awni Y Hannun, and Andrew Y Ng. “Rectifier Nonlinearities Improve Neural Network Acoustic Models”. In: *ICML Workshop on Deep Learning for Audio, Speech, and Language Processing (WDLASL 2013)*. 2013.
- [70] Scott C. Douglas and Jiutian Yu. “Why RELU Units Sometimes Die: Analysis of Single-Unit Error Backpropagation in Neural Networks”. In: *2018 52nd Asilomar Conference on Signals, Systems, and Computers*. Pacific Grove, CA, USA: IEEE, 2018-10, pp. 864–868.
- [71] Martín Abadi et al. *TensorFlow: Large-scale Machine Learning on Heterogeneous Systems*. 2015.
- [72] Vladimir B. Braginsky, Farid Ya Khalili, and Kip S. Thorne. *Quantum Measurement*. en. Google-Books-ID: 42xfQgAACAAJ. Cambridge University Press, 1992-09.
- [73] A. R. Mills et al. “Shuttling a single charge across a one-dimensional array of silicon quantum dots”. en. In: *Nat Commun* 10.1 (2019-03). Publisher: Nature Publishing Group, p. 1063.
- [74] K. S. Kumar et al. “Stimulated Raman adiabatic passage in a three-level superconducting circuit”. en. In: *Nat Commun* 7.1 (2016-02). Publisher: Nature Publishing Group, p. 10628.
- [75] H. K. Xu et al. “Coherent population transfer between uncoupled or weakly coupled states in ladder-type superconducting qutrits”. en. In: *Nat Commun* 7.1 (2016-03). Publisher: Nature Publishing Group, p. 11018.
- [76] Musang Gong et al. “Two-Photon-Transition Superadiabatic Passage in a Nitrogen-Vacancy Center in Diamond”. In: *Phys. Rev. A* 109.3 (2024-03), p. 032626.
- [77] Jens Siewert, Tobias Brandes, and G. Falci. “Advanced control with a Cooper-pair box: Stimulated Raman adiabatic passage and Fock-state generation in a nanomechanical resonator”. In: *Phys. Rev. B* 79.2 (2009-01). Publisher: American Physical Society, p. 024504.
- [78] G. Falci et al. “Design of a Lambda system for population transfer in superconducting nanocircuits”. In: *Phys. Rev. B* 87.21 (2013-06). Publisher: American Physical Society, p. 214515.

- [79] N. Earnest et al. “Realization of a Λ System with Metastable States of a Capacitively Shunted Fluxonium”. In: *Phys. Rev. Lett.* 120.15 (2018-04). Publisher: American Physical Society, p. 150504.
- [80] P. G. Di Stefano et al. “Coherent manipulation of noise-protected superconducting artificial atoms in the Λ scheme”. In: *Phys. Rev. A* 93.5 (2016-05). Publisher: American Physical Society, p. 051801.
- [81] G Falci et al. “Effects of Low-Frequency Noise in Driven Coherent Nanodevices”. In: *Phys. Scr.* T151 (2012-11), p. 014020.
- [82] B. Spagnolo et al. “Relaxation Phenomena in classical and Quantum systems”. en. In: *Acta Phys. Pol. B* 43.5 (2012), p. 1169.
- [83] Alexandre Blais, Steven M. Girvin, and William D. Oliver. “Quantum information processing and quantum optics with circuit quantum electrodynamics”. en. In: *Nat. Phys.* 16.3 (2020-03). Publisher: Nature Publishing Group, pp. 247–256.
- [84] G. Falci et al. “Ultrastrong coupling probed by Coherent Population Transfer”. en. In: *Sci Rep* 9.1 (2019-06). Publisher: Nature Publishing Group, p. 9249.
- [85] L. Giannelli et al. “Detecting virtual photons in ultrastrongly coupled superconducting quantum circuits”. In: *Phys. Rev. Res.* 6.1 (2024-01). Publisher: American Physical Society, p. 013008.
- [86] P. G. Di Stefano et al. “Population transfer in a Λ system induced by detunings”. In: *Phys. Rev. B* 91.22 (2015-06). Publisher: American Physical Society, p. 224506.